Automatic extraction of brain surface and mid-sagittal plane from PET images applying deformable models

J Mykkänen [a] J Tohka [b] J Luoma [b] U Ruotsalainen [b]

[a] *Department of Computer and Information Sciences, FIN-33014, University of Tampere, Finland. E-mail: jouni.mykkanen@cs.uta.fi. Tel: +358-3-2156193. Fax: +358-3-2156070.*

[b] *Institute of Signal Processing, Tampere University of Technology, Finland*

Abstract

In this study, we propose new methods for automatic extraction of the brain surface and the mid-sagittal plane from functional positron emission tomography (PET) images. Designing general methods for these segmentation tasks is challenging because the spatial distribution of intensity values in a PET image depends on the applied radiopharmaceutical and the contrast to noise ratio in a PET image is typically low. We extracted the brain surface with a deformable model which is based on global minimization of its energy. The global optimization allows reliable automation of the extraction task. Based on the extracted brain surface, the mid-sagittal plane was determined. Since we did not apply information from the corresponding anatomical images, the extracted brain surface and mid-sagittal plane could be used also when registering PET images to anatomical images. Furthermore, we applied the deformable model for extraction of the coarse cortical structure based on the tracer uptake from FDG-PET brain images. We tested the methods with the image of the Hoffman brain phantom (FDG) and images from brain studies with FDG (17 images) and ^{11}C-Raclopride tracers (4 images). The brain surface, the mid-sagittal plane, and the cortical structure were reliably delineated from all the images without any user guidance. The proposed segmentation methods provide a promising direction for automatic processing and analysis of PET brain images.

Key words: brain surface extraction, segmentation, mid-sagittal plane

1 Introduction

Positron emission tomography (PET) can be used to study biochemical processes involved in living organs like the brain. Segmentation of, or extraction of volumes of interest (VOI) from PET images is important for regional quantification. Entirely manual methods are not practical for segmentation of a large set of PET images because it is time-consuming work where individual human analyzers produce a lot of variance in the results. Thresholding and clustering techniques could be applied, but they require user-interaction and manual editing of the extracted volumes of interest. A standard procedure to delineate structures according to their surfaces from PET brain images is to segment the corresponding anatomical magnetic resonance (MR) images and then to superimpose the found anatomical surfaces on the PET images (Huesman et al., 1998). In that study, Huesman et al performed coregistration between PET and MR images manually because obviously a very accurate registration is required. Automatic image registration is not a trivial task due to initial incongruity of structure and function and fundamental differences between PET images acquired with different radiopharmaceuticals. For more about the image registration methods available for nuclear medicine we refer to the recent survey (Hutton et al., 2002).

The biochemical process described by a PET image is defined by the applied radiopharmaceutical from which also the spatial distribution of intensity values in the image depends on. Furthermore, PET images are typically noisy. Therefore, designing automatic and generally applicable methods even for extraction of the brain surface is a challenging task. Nevertheless, automatic brain surface extraction is a desirable aim. The brain surface can be used, as we demonstrate in this paper, for determination of the mid-sagittal plane. Also, reliable delineation of the brain surface from various kinds of PET brain images opens up new possibilities for performing image registrations between PET and anatomical images by applying, for example, the iterative closest point algorithm (ICP) (Besl and McKay, 1992; Zhang, 1994; Ardekani et al., 1995). Obviously, this requires processing of PET images without relying on information from the corresponding anatomical MR images. In a similar way the brain surface, and perhaps the mid-sagittal plane could be used for compensating patient movement during a dynamic PET study or patient mispositioning between PET studies.

If other brain structures could be extracted reliably both from PET and MR images, also they could be used as a basis for registration and patient motion compensation. By a structure in a PET image we mean a volume in the image, which has distinguishable (positive) uptake of the radiopharmaceutical from its surroundings. We have addressed brain structure extraction within PET in earlier studies. The thresholding method for extracting structures interactively from the PET brain images was studied in (Mykkänen et al., 2000). A sagittal slice was interactively determined from PET image to separate the image into two parts roughly corre-

sponding the two hemispheres to be able to set thresholds for both parts separately. This simple method was applied to extract the structures corresponding the left and the right striatum from FDOPA-PET images. We have also examined two-dimensional (2D) generalized snakes (g-snakes) (Lai and Chin, 1995) for extraction of the structure corresponding cortex from selected planes of FDG-PET brain images in (Mykkänen et al., 2001). However, while the results obtained with g-snakes were encouraging, it was impossible to use the 2D method to process the three-dimensional image volumes automatically. Besides, we applied also information from the corresponding MR image for segmentation and therefore use of segmentations for registration purposes would be problematic.

In this study, we propose an automatic method for extraction of the brain surface from FDG and Raclopride PET images. The extraction is based on a new three-dimensional deformable surface model developed in our research group (Tohka and Mykkänen, 2003). An important property of the deformable model is its low sensitivity to its initialization achieved by global minimization of its energy. This allows generation of initializations completely without user guidance, which is important if a large set of images is to be processed. Based on the found brain surface, we continue by determining the mid-sagittal plane. We consider also extraction of a structure corresponding cortex from FDG-PET images using the deformable model. All proposed methods are relying on data only from PET images themselves and therefore delineated surfaces could be used for registration purposes. Some surface extraction results with FDG-PET images have been presented previously in (Ruotsalainen et al., 2001) and (Mykkänen et al., 2003). Preliminary experiments for extracting the mid-sagittal plane from FDG-PET brain images have been presented in the abstract (Luoma, 2002).

2 Background

2.1 PET images

Positron emission tomography provides a unique method to investigate physiological processes in the brain. The distribution of the intensity values in a PET image depends on the applied radiopharmaceutical. For example the receptor type tracers, like Raclopride, have uptake mainly in the structures having the highest densities of the corresponding receptors, whereas the tracers describing metabolic functions like FDG, which is the tracer for glucose consumption, have uptake all over the brain area, and the highest uptake in the cortical region. A functional structure in a PET image can be defined as a volume having distinguishable different, normally higher intensity values than its surroundings. Low contrast to noise ratio in the PET images causes problems for those segmentation methods, which are based only on intensity values. Figure 1 presents the intensity histograms of one of the FDG-PET

and one of the Raclopride PET brain images collected for this study. From the histograms it is clear that the voxels in a PET brain image cannot be classified similarly as the voxels in anatomical MR images because there is no grouping of intensity values around some structure bound mean value. Thus, the use of intensity-based segmentation methods needs interaction in the definition of meaningful threshold values for extraction of volumes of interest (VOI). For automatic extraction, a more advanced segmentation method is required which should be resistant to noise and it should also be able to deal with the whole functional structure. This can be achieved if also a priori information of the approximate position and size of the object to be searched for can be included in the segmentation process.

The quality of PET images depends on the applied image reconstruction method. The positron emission data acquisition is subject to a substantial amount of statistical noise, originating from the statistical nature of the decay of the positron emitting isotope used for labeling the tracer molecule. The conventional filtered back-projection image reconstruction produces images with noise and reconstruction artifacts. The iterative image reconstruction methods, especially those including noise regularisation in the reconstruction process produce better image quality. We have introduced iterative median root prior reconstruction method (MRP), which has shown to produce outstanding noise reduction properties without blurring the edges in the images (Alenius and Ruotsalainen, 2002). It is obvious that improved image quality, especially sharp edges and controlling of the noise content, helps the segmentation of PET images.

2.2 Deformable models

Deformable surface models are advanced methods for image segmentation and surface extraction. They use prior information about geometry of objects of interest in addition of image data. Therefore, they are not as sensitive to imperfections in image data as segmentation methods which rely solely on image data. As a consequence, deformable models have found various applications within analysis of medical images (McInerney and Terzopoulos, 1996).

A deformable model consists a geometric representation of a surface and evolution rules that control the adaptation of the surface shape according to the image data. The shape adaptation is often formulated as an energy minimization problem. The energy function of a deformable surface model consists of an external energy term derived from image data and an internal energy term which depends only on the properties of surfaces themselves. A common drawback of deformable models is that the formulated energy minimization problem is difficult to solve due to numerous local minima. This easily leads to problems with the initialization of deformable models. In other words, the initial surface has to be in a close vicinity of the target surface in order for a standard deformable model to converge to a

correct solution. There exist several advanced methods that have been proposed to solve the initialization sensitivity problem, but reviewing these would be outside of the topic in this study.

Deformable models for MR brain images

Deformable models have been used extensively for analysis of three-dimensional MR brain images. We review briefly a few applications of them and point out their differences to processing of PET images.

Extraction of cerebral cortex from MR images is a difficult task because the complex shape of the cortex is problematic to capture properly. MacDonald et al. (2000) considered automatic extraction of inner and outer surfaces of cortical gray matter from MR images. They first classified voxels in a MR image according to their tissue type. Thereafter, a deformable surface based on simple coarse-to-fine optimization was used to locate boundary between grey and white matter, the inner surface of the cerebral cortex. Starting from the inner surface of cortex and applying proximity constraints, the outer surface of the cortex was extracted. The method depends on voxel classification and therefore it is not directly applicable for PET images.

Xu et al. (1999) proposed to use a generalized gradient vector flow (GGVF) - based deformable model (Xu and Prince, 1998) to obtain a representation of the central layer of the cerebral cortex. They also first classified images according to the tissue types and then generated initializations for deformable surfaces based on voxel classifications. The initialization stage required some user interaction. GGVF deformable models do not necessarily require voxel classification prior to their application. Also other researchers have considered extraction of cerebral cortex from MR images (Davatzikos and Bryan, 1996; Zeng et al., 1999; Vaillant and Davatzikos, 1997).

Shen et al. (2001) extracted ventricles and nuclei from MR brain images using a deformable surface model. They relied on edge-detection instead of voxel classification in the formulation of the external energy for their deformable model. However, they applied rather complex shape modeling scheme requiring hand-crafted example surfaces.

Deformable models for PET images

Deformable surface models are attractive methods for analysis of anatomical MR images. Due to differences between PET images and MR images explained in Section 2.1, direct application of deformable models designed for MR images is not necessarily plausible for analysing PET image data. However, deformable models have been considered also within PET and SPECT (single photon emission

computed tomography) although not as extensively as within MR imaging. Also, within PET or SPECT, most of the applications of deformable models seem to focus on cardiac images. Bardinet et al. (1998) used deformable models for extraction of the left ventricle of the heart from cardiac SPECT images. The deformable model combined superquadrics with few degrees of freedom to free form deformations in order to properly segment noisy images. The method relies on thresholding of images and the selection of the threshold value appears to require user-guidance. Noumeir and El-Daccache (1998) applied a 3D generalization (Cohen and Cohen, 1993) of the snakes algorithm (Kass et al., 1987) for attenuation correction with cardiac SPECT images. However, based on the short description of the algorithm it is hard to deduct the level of automation of their method. Deformable motion algorithm was presented in (Klein and Huesman, 2002) to compensate for patient motion in gated PET cardiac images. However, as this problem is quite different from ours, we do not consider it further here. In (Debreuve et al., 2001), level-set based deformable models (Malladi et al., 1995) were applied to segmentation of 4D (3D and time) gated myocardial SPECT images. In our applications it is favorable to constrain topologies of the extracted surfaces and therefore level set techniques are of limited interest for us.

Tohka (2002) has studied brain surface extraction from PET images using different deformable models. A preliminary version of the deformable model applied in this study was featured in the study. Tohka concluded that the problem seems to be hard if automatic use of deformable models is desired. However, two deformable models, the one considered in this study and the GGVF-based model (Xu and Prince, 1998) mentioned already, yielded good extraction results. Of course, as stated in (Tohka, 2002)the results of such a study are open to many interpretations and drawing too strict conclusions about superiority of one method over the others for the task should be avoided.

2.3 Extraction of mid-sagittal plane from PET brain images

Difference in brain function between the two hemispheres is an interesting topic for a neurological study. To study it, hemispheres of the brain must be coarsely separated in a brain image. This can be done by identifying the mid-sagittal plane of the brain. The mid-sagittal plane can be defined as the one plane about which the reflective symmetry of the brain is maximized in the image. Several measures have been used as the symmetry criterion within PET. Ardekani et al. (1997) considered the cross-correlation of the intensity values between hemispheres as the symmetry criterion. This criterion is obviously sensitive to asymmetries and anisotropy of intensity values between hemispheres. Prima et al. (2002) used block-matching and robust regression techniques to find the mid-sagittal plane even when there exist normal or abnormal asymmetry in the brain.

Also, symmetry criteria that are not directly related to intensity values can be considered. Liu et al. (2001) considered the symmetry of edge-images rather than symmetry of the original intensity images. They applied their method only for anatomical MR or CT images. In this study, we extend their method for functional PET images. However, it could be expected that edge-images would not have a quality good enough for reliable determination of the mid-sagittal plane. Therefore, we base our mid-sagittal plane extraction algorithm to PET brain surfaces that are extracted by the deformable surface model.

3 Deformable surface model

Surfaces are extracted from volumetric images by minimizing the energy function of the deformable model. Surfaces are approximated by simplex meshes (Delingette, 1999). A set of discrete points $\mathbf{W} = \{\mathbf{w}_1, \mathbf{w}_2, \ldots, \mathbf{w}_n\}$, called mexels ($\in \mathbb{R}^3$), and adjacency relations between mexels define a simplex mesh. Adjacency relations are known and constant, hence symbol $\mathbf{W}$ is used for a simplex mesh.

3.1 Energy model

The total energy of the surface mesh $\mathbf{W}$ is defined as

$$\begin{aligned} E(\mathbf{W}) &= \lambda E_{int}(\mathbf{W}) + (1-\lambda) E_{ext}(\mathbf{W}) \\ &= \frac{1}{n} \sum_{i=1}^{n} \Big(\lambda E_{int}(\mathbf{w}_i) + (1-\lambda) E_{ext}(\mathbf{w}_i) \Big). \end{aligned} \tag{1}$$

The regularisation parameter λ is in range $[0, 1]$. The external energy E_{ext} couples $\mathbf{W}$ to the salient image features. The internal energy E_{int} regularizes the shape of the surface.

The internal mexel-wise energy is defined as

$$E_{int}(\mathbf{w}_i) = \frac{\| \mathbf{w}_i - \alpha \sum_{j=1}^{3} \mathbf{w}_{i_j} \|^2}{A(\mathbf{W})}, \tag{2}$$

where $\mathbf{w}_{i_j}$ are the neighbouring mexels of $\mathbf{w}_i$ in the mesh, $A(\mathbf{W})$ is the average area of the faces of the mesh, and α is the shape parameter. For the thin-plate shape model

$$\alpha = \frac{1}{3} \tag{3}$$

and for the sphere shape model (Tohka and Mykkänen, 2003)

$$\alpha = \left(3\cos\left(2\arctan\frac{2(\sqrt{\pi\sqrt{3}})}{3(\sqrt{n})}\right)\right)^{-1}. \quad (4)$$

The sphere shape model is more complicated, but applying it often leads better results than applying the simpler thin-plate shape model.

The precise form of the external energy function depends on the applied tracer because different image-features characterize surfaces of interest with different tracers. Therefore, for notational simplicity, we define the external energy with the help of energy images. An energy image is generated from the image to be processed in such a way that intensity values in the energy image describe saliency of voxels for the application and the tracer. The external energy at the position $\mathbf{w}$ is

$$E_{ext}(\mathbf{w}) = 1 - B(\mathbf{w}), \quad (5)$$

where B is *the energy image*. Energy images are normalized to have intensity values from 0 to 1. The generation of the energy images based on the original images is explained in Section 4.1.

3.2 Energy minimization

The energy function (1) is likely to have multiple local minima. Therefore, global minimization of it is necessary to render the deformable model insensitive to its initialization. We proposed an effective dual surface minimization (DSM) algorithm for the global optimization task in (Tohka and Mykkänen, 2003). The algorithm is based on the iterative optimization of two surface meshes, which approach the surface of interest from different directions. We name the energy based deformable model (DM) with the DSM algorithm as *the DM-DSM method*.

Standard DSM algorithm

The DSM algorithm begins with two meshes: the outer mesh and the inner mesh. These are created from a given initial mesh preserving its properties, except the size. Their sizes are set in such a way that the surface of the searched structure lies in the space between them. This is *the search volume* for the minimization process.

The search is based on the iterative minimization of the energies of the outer and inner surfaces. The energies for the both surfaces are calculated from equation (1). During each iteration, the energy of the mesh is minimized using a greedy method adapted from (Williams and Shah, 1992). It is used in such a way, that the

outer surface shrinks and the inner surface grows. After each iteration, the DSM algorithm compares the energies of the outer and inner surfaces and continues minimization from the surface having higher energy. If the surface having higher energy gets stuck in a local energy minimum, the energy of the current surface position is increased until the surface moves again. The DSM algorithm is stopped when the volume inside of the inner surface exceeds the volume inside the outer surface. The algorithm selects the surface having the lower energy as the result.

DSM-OS algorithm

Sometimes, for example when extracting brain surfaces from PET images, it is favorable to approach the surface of interest from outside. The reason for this with PET brain surface extraction is that energy images usually contain more noise inside the brain volume than outside of it. For situations like this, we have developed a DSM-OS (DSM - outer surface) variant from our optimization algorithm. The DSM-OS algorithm uses only one surface mesh approaching the target from outside. The modification is straight-forward to implement. Instead of comparing the outer mesh to the inner mesh as with the standard algorithm, the energy of the current outer mesh is compared to the lowest energy already found. The iterative algorithm is stopped when the volume of the (outer) surface mesh becomes smaller than a given threshold. For more details about the variant and advantages of it for brain surface extraction from PET images see (Tohka and Mykkänen, 2003).

4 Surface Extraction from PET Brain Images

In this Section, we describe how the DM-DSM method has been implemented to extract surfaces automatically from PET brain images. Determination of the mid-sagittal plane is performed using the extracted brain surfaces. A flowchart of the procedure is presented in Figure 2.

4.1 Computation of energy images

FDG-PET

As mentioned earlier, intensity values in an energy image should ideally be high at the voxels belonging to surface of interest and low elsewhere in the energy image. With FDG, edges in original images seem to be a good and simple feature characterizing surfaces of interest. We define the energy image for FDG as

$$B_{FDG} = ||\nabla MF(I)||, \tag{6}$$

where I is the FDG-PET image to processed and MF denotes a median filter. The gradient is computed by the three-dimensional Sobel operator (Zucker and Hummel, 1981). In practise, the energy image B_{FDG} can contain few aberrantly large intensity values, which reduce the contrast in other parts of the image. Therefore, to improve the contrast, a certain (small) percentage of largest intensity values all receive intensity value 1 in the normalized version of the energy image. The steps for computing B_{FDG} are depicted in Figure 3.

Raclopride PET

For brain surface extraction from Raclopride PET images, constructing energy images requires somewhat more effort than in the case of FDG-PET images. The whole process is depicted in Figure 4. As can be seen from Figure 4 (a), the highest tracer uptake present in the images is within the striatum and tracer uptake elsewhere in the brain volume is rather low. Therefore, after median filtering the Raclopride images, we determine which voxels are likely to belong to the striatum. The determination is based on the expected volume of the striatum and the assumption that the striatum consists of voxels with the highest intensity values in the image. Intensity values within the so-determined striatum are then replaced by the average intensity value of the image, cf. 4 (c). This way we need not to be concerned about voxels which have been incorrectly classified as those belonging to the striatum. After this, we apply a gray-level morphological opening with a flat and symmetric structuring function to the image (Heijmans, 1991).

After the preprocessing steps (Figure 4 (d)), it can be seen that voxels just outside the brain volume have low intensity values. Also, their values in the gradient magnitude image are relatively high. Hence, we set

$$B_{Raclopride}(\mathbf{x}) = ||\nabla I_F(\mathbf{x})||(1 - I_F(\mathbf{x})), \tag{7}$$

where $B_{Raclopride}$ is the energy image for Raclopride PET images and I_F (as in Figure 4 (d)) denotes the pre-processed image. Intensity values of I_F are normalized to lie in the range $[0, 1]$ and the gradient is computed as with the FDG images. To improve the contrast of the energy images, we scale down largest intensity values present in the energy image similarly as with FDG-PET images.

4.2 Delineation of the brain surface

In the energy image (Figures 3 (d) and 4 (f)), the brain surface has relatively high contrast against background. Also, the noise level outside of the brain volume is considerably lower than inside of it in the energy image. Hence, we apply the DSM-OS modification approaching brain surface from outside for extraction of it.

For automatic generation of the initialization for the deformable model, we assume that the centre point of the brain is located near the mass centre of voxel intensities in the original image. A large, as compared to image dimensions, ellipsoid is used as the initial surface. The centre of the ellipsoid is set into the mass centre of voxel intensities. An example of this kind of initialization is shown in Figure 5. From this, the DM-DSM method (using DSM-OS algorithm) delineates the surface of brain. The thin-plate shape model is used in the brain surface extraction. The reason for this is that the location of the brain in the image is relatively unknown prior to the extraction process and the internal energy with the sphere shape model is not translation invariant, see (Tohka and Mykkänen, 2003).

4.3 Determination of the mid-sagittal plane

For extraction of the mid-sagittal plane, we applied an existing edge-based method originally designed for anatomical brain images (Liu et al., 2001). However, as the contrast to noise ratio of PET images is rather low, we apply the extracted brain surfaces instead of the edge-images as the basis for mid-sagittal plane extraction. Hence, we define the mid-sagittal plane as the one about which the reflective symmetry of the brain surface is maximized.

The algorithm used in this study is highly similar to the one described in (Liu et al., 2001) and therefore we describe it here only briefly. The algorithm first determines the slope of the symmetry axis on each axial slice of the image. This is done by maximizing with respect to θ the cross-correlation between the brain contour on that slice rotated by angle θ and vertically reflected version of the brain contour rotated by angle $-\theta$. Brain contours are intersections of the brain surface and axial image cross-sections. Thereafter, the slopes of the symmetry axes on each slice are combined to yield an estimate $\hat{\theta}$ of the common slope of the intersection of the mid-sagittal plane and transaxial cross-sections by using a robust estimation technique. Once we have obtained the estimate $\hat{\theta}$, offsets of the mid-sagittal plane to the symmetry axis defined by $\hat{\theta}$ on each slice can be computed again by maximizing cross-correlation of the brain contours on each axial slice. Based on these offsets robust least median of squares regression (Rousseeuw and Leroy, 1987) is used to determine remaining parameters required for specifying the mid-sagittal plane. See (Liu et al., 2001) for more detailed explanation of the algorithm.

4.4 Extraction of the white matter surface

We apply the standard DSM-algorithm for extraction of the white matter surface. The white matter surface is the boundary between the tracer uptake levels in gray matter and white matter tissues that is visible in FDG-PET images. The delineated white matter surface together with the brain surface defines the coarse cortical

structure in the image. However, before proceeding with surface extraction, we remove high intensity values relating to the brain surface from the energy image. This is done based on the previously extracted brain surface. The already found brain surface can also be used for generating initializations for the DSM algorithm. The inner and outer initial surfaces are created from it by scaling. Both shape models, the thin-plate and the sphere, can be applied to the extraction of the white matter surface.

5 Material: PET studies

Brain surface extraction and determination of the mid-sagittal plane were evaluated with images from a phantom study and images from ^{18}FDG-PET and ^{11}C-Raclopride PET studies of healthy volunteers. The white matter surface was extracted from the phantom images and the FDG images. The Hoffman brain phantom (JB003, Nuclemed N.V./S.A., Roeselare, Belgium) was filled with ^{18}FDG. Structures corresponding to cerebellum, cortex, basal ganglia and ventricles are represented in the phantom.

All the PET acquisitions were made with GE Advance scanner (GE, Milwaukee, USA). The FDG-PET images were reconstructed with the iterative MRP method to the cross-section image size of 128 by 128 (Alenius et al., 1998). The voxel size was $1.72mm \times 1.72mm \times 4.25mm$. The Raclopride PET images were reconstructed with the FBP method to the same size than the FDG images. The voxel size was $2.3mm \times 2.3mm \times 4.25mm$.

From the phantom study we created two images where the brain was in two different orientations, mainly to test the algorithm for determining the midsagittal plane. In one image, the brain was in the neurological orientation and in the other it was slightly rotated from this orientation. The resulting images are called the original phantom and the rotated phantom, respectively. The rotation was implemented using AIR software (Woods et al., 1993), and the rotation angles were 3° in the transaxial plane (yaw), 0° in the sagittal plane (pitch) and 5° in the coronal plane (roll). Rotations were performed in the order yaw, pitch, and roll.

The pixel by pixel Patlak model was applied to the FDG sinograms to produce parametric images to be used in the delineation process (Ruotsalainen, 1997). The Raclopride images were calculated to parametric images showing the Raclopride binding with a simplified reference model (Gunn et al., 1997).

For parameters for the surface extraction method, ranges of values evaluated with the phantom study were based on our earlier experiments in (Mykkänen et al., 2003). Surface extraction was tested with meshes of 320, 960 and 1280 mexels. The value of regularisation parameter λ was varied in the range 0-0.5 for the search. Ex-

traction of the white matter surface, where we apply the standard DSM-algorithm, was performed with two types of initializations: initial surfaces were generated from an ellipsoid or from the extracted brain surface. These called, respectively, the ellipsoid initialization and the brain surface initialization. The thin-plate and the sphere prior shapes were tested for the white matter surface extraction. The evaluation was based on visual comparison of the extracted surface to the energy image and the original image. The parameter values from the phantom study were used for extraction of surfaces from images seventeen FDG and four Raclopride brain studies.

6 Results

6.1 Phantom study

Brain surface

The accuracy of the extracted brain surfaces was excellent when it was visually compared against the energy images as well as against the original images. The brain surface extracted from the rotated image is shown in Figure 6 and the brain surface extracted from the original is shown in Figure 7. The initialization for the DSM-OS in the case of the original image was the one shown in Fig. 5. As can be seen from Figures 6 and 7, there were no differences between visual qualities of the brain surface extracted from the original phantom image and the brain surface extracted from the rotated image. The extracted surfaces matched well with all surface details present in energy images. Particularly, the surface concavity at lower parts of the brain surface was captured properly, as can be seen from the coronal cross-section in Figure 6.

Positioning of initial (ellipsoid) surfaces according to the mass centre of image intensities was found to be an appropriate method for initializing the DSM-OS algorithm. The DSM-OS algorithm was not sensitive to the size of the initial surface as long the surface of interest was located inside of it.

The number of mexels in a mesh should be sufficiently large for representing the surface to be extracted. The mesh size of 1280 mexels was found to be appropriate for extraction of the brain surface. Details of the brain surface visible in images were properly captured with this mesh resolution. Meshes comprising of 320 or 960 mexels could not accurately represent the brain surface.

In Equation (1), the parameter λ defines relative weights of the internal energy and of the external energy. The brain surface was properly found with the evaluated range of values of parameter λ (0.05-0.5) and the DSM-OS algorithm was found

to be rather insensitive to the value of λ in this case. We selected the value 0.3 from the evaluated range for the use with the phantom images. However also other choices would be possible, because the extracted surfaces with different values of λ were highly similar. For the reasons explained in Section 4.2, the brain surface was extracted only using the thin-plate shape model.

Mid-sagittal plane

The mid-sagittal plane extracted from the original as well as the rotated phantom images was in a proper position and orientation when visually compared to the images. Intersections of the extracted mid-sagittal planes from the phantom images with transaxial and coronal image cross-sections are shown in Figure 6.

White matter surface

The white matter surface was extracted with the ellipsoid and the brain surface initializations. The accuracy of delineated surfaces was comparable to the quality and the resolution of images with both initializations. However, with the ellipsoid initialization the DM-DSM method expressed sensitivity to the size of the inner initial surface mesh. Therefore, for automatic surface extraction, initializations generated based on the extracted brain surfaces would be the safer choice. The extracted white-matter surfaces from phantom images with the brain surface initialization are shown in Figure 6. With the brain surface initialization, the DM-DSM method was rather insensitive to the size of the search volume. The mesh size of 1280 mexels was found to be appropriate to capture the white matter surface from the phantom images. By using meshes of 320 or 960 mexels, the accuracy of the extracted surfaces was compromised by an insufficient mesh resolution. Both shape models, the thin-plate and the sphere, were examined for segmentation of the white matter surface. Extracted surfaces with the sphere shape model were slightly better in visual inspection.

The search process was more sensitive to the value of λ with the white matter surface than with the brain surface. Examples of the effect of the change of this value are shown in Figure 7. The sphere shape model was applied in these tests. If the shape regularisation was omitted ($\lambda = 0$), the DM-DSM method produced bumpy surfaces attracted by high intensity peaks in the energy image. An example is shown in Figure 7 (a), where the transaxial cross-section of the white matter surface seems to be of rather good quality, except for peaks of the surface visible near the middle of the image cross-section. The 3D rendering of the same surface in Figure 7 (a) better reveals that omitting shape regularisation compromises the smooth appearance of the resulting surface. Consequently, shape regularisation is needed for proper extraction of the surface. On the other hand, setting λ to 0.5 led to over-regularisation as can be seen from Figure 7 (d). Extracted white matter

surfaces with values of λ set to 0.05 and 0.2 are depicted in Figures 7 (b) and (c). Although these two surfaces are clearly different, they are hard to rank. It seems that appropriate values for parameter λ are from 0.05 to 0.2. This was the case with both shape models. The white matter surfaces in Figure 6 were both extracted with $\lambda = 0.2$.

6.2 FDG and Raclopride brain studies

From the phantom tests, we obtained the parameter values for the evaluation of the DM-DSM method in the case the FDG and Raclopride brain studies. The mesh size of 1280 mexels was applied for all surfaces.

Brain surface

The brain surfaces delineated from all 17 FDG-PET images were of excellent quality. In Figure 8, examples of cross-sections of extracted brain surfaces from FDG-PET images are overlayed on the corresponding energy images. In Figure 9, same surface cross-sections divided to left and right hemispheres are overlayed on the original FDG-PET images. Magnifications (by 500%) from the transaxial cross-sections in Figure 8 show how the extracted brain surfaces follow the details visible in the energy images. In Figure 10, 3D renderings of the three extracted brain surfaces depicted in Figure 9 are shown together with the determined mid-sagittal planes.

The visual quality of brain surfaces extracted from Raclopride images was nearly as good as with FDG images. However, with the Raclopride PET images, the accuracy of extracted brain surfaces was quite difficult to evaluate because brain volumes are barely visible in the original images. Figure 11 presents one example of the extracted brain surface from Raclopride studies overlayed (a) on the original image, (b) on the median filtered image and (c) on the energy image. From the figure, it can be seen that the DM-DSM method was able to capture boundary concavity at lower parts of the brain remarkably well. In three cases out of the four studied, the delineated surfaces were of similar quality as the one depicted in Figure 11. Only in a single case out of the four there were minor but clear errors in the delineated surface. These errors were explainable by imperfections in the energy image.

As with the phantom studies, positioning the initial (ellipsoid) surface according to the mass centre of intensity values in the images was found to be an appropriate method to generate initializations for the DSM-OS algorithm. Due to individual variations in the size of the brain, practically the whole image volume needs to be inside the initial ellipsoid for automatic search. This did not present any problems for the DSM-OS algorithm, although initializations were quite far from the surfaces of interest. The thin-plate shape model was used for the search of the brain surface

as with the phantom study. The effect of the value of the parameter λ was found to be minimal in extraction of the brain surface in the human studies. The same value ($\lambda = 0.3$) as with the phantom study was chosen. All the brain surfaces from FDG-PET and Raclopride PET images in Figures 8, 9, 10 and 11 were extracted using this value of the parameter.

The steps required for generation of the energy images with the Raclopride tracer were different from those with the FDG tracer. The distinct uptake of this kind of receptor tracers concentrates almost only in striatum and the other areas of the brain image remain almost invisible and have a very low contrast to the background. In pre-processing, the removal of the striatum was needed for defining a proper energy image for the search of the brain surface. The volume of striatum was always overestimated. This did not cause any problem for the search, since the intensity values of the volume were replaced with the average intensity value of the image. Although the needed image processing was a bit more complicated with the Raclopride images than with FDG images, we could apply exactly the same processing steps for all the four Raclopride images without user interaction.

Mid-sagittal plane

The mid-sagittal plane was automatically determined based on the extracted brain surfaces for all 17 FDG-PET and 4 Raclopride PET images. The extracted mid-sagittal planes are depicted on transaxial and coronal cross-sections in Figures 8, 9 and 11. The position and orientation of the mid-sagittal plane was proper in visual inspection with every image. Especially, minor errors in the extracted brain surface from one of the Raclopride images did not compromise the robustness of mid-sagittal plane determination.

White-matter surface from FDG images

For the white matter surface, the found brain surface was used for generating the initial surfaces for the standard DSM algorithm. Because the noise level in the FDG brain images was significantly higher than in the phantom image, we tested white matter surface extraction with different values of the parameter λ also in this case. The best value of λ was found to be 0.2 (tested range 0.05-0.4). However, the difference to the phantom study was that smaller values of λ the quality of results clearly degraded from those obtained with $\lambda = 0.2$.

The visual quality of delineated surfaces varied more with the white matter surface than with the brain surface. The example images shown in Figures 8 and 9 were chosen and ranked based on the visual quality of the extracted white matter surfaces. The delineated surface of the best accuracy, subject 1, followed the white matter surface details slightly better than the result surface of typical quality, subject 2. In the worst case, subject 3, the extracted surface had a clear spike diverging

from ‘the correct’ white matter surface. This spike can be seen on top of the sagittal cross-section view in Figure 8. However, there were no clear differences in the visual quality of the delineated surfaces when they were compared to the energy images, see the magnifications in Figure 8. The difference in goodness between the best and typical surfaces was quite marginal and the ranking is therefore highly subjective. The division of the cortical VOIs into left and right hemispheres based on the mid-sagittal planes is depicted in Figure 9.

6.3 Summary of Results

The brain surfaces were automatically extracted from two completely different types of PET images: FDG-PET images and Raclopride PET images. The surface extraction process was the same for all images, except for pre-processing of images. All brain surfaces were accurate in visual inspection as compared to the image resolution. Especially boundary concavities within lower parts of brain surfaces were captured properly. Determination of the mid-sagittal plane was automatic for all images. This task could be challenging for Raclopride images if only image intensity values were to be used for it. Combining the brain surface, the mid-sagittal plane and the white matter surface, we were able to determine the left cortical and the right cortical VOIs from the PET-FDG images without user interactions, see transaxial and coronal cross-sections in Figure 9.

7 Discussion

We have applied a deformable model based DM-DSM method for demanding surface extraction problems arising with functional positron emission tomography (PET) brain images. In this study, we demonstrated that the brain surfaces for both FDG and Raclopride images could be automatically delineated with the new global optimization-based deformable model. The surface extraction procedure and the parameters for the deformable model were the same with both radiopharmaceuticals, only the definitions of the energy images differed. The extracted brain surfaces were found to follow quite accurately the brain surfaces when compared to the original PET images as well as to the corresponding energy images. The brain surface provided a good basis for searching other surfaces from brain images. We applied the delineated brain surfaces for determination of the mid-sagittal plane of the brain for all the images. Together with brain surface visualization, the mid-sagittal plane helps in orientation in the three-dimensional brain image set for image registration purposes or for determination of volumes of interest. The extracted brain surface and white matter surface from FDG images made possible to determine the cortical volumes of interest (VOIs) automatically from FDG images. With the found mid-sagittal planes these VOIs can be divided in two parts representing

the two hemispheres. Although this may not be the sufficient way to delineate the gray matter volume from FDG-PET brain images, where the tracer uptake is highest in cortex, it shows that even with this kind of limited image quality there are possibilities to apply automatic means for surface extraction and determination of volumes of interest.

Deformable surface models are methods that can extract geometrically continuous structures from noisy volumetric images. Surface extraction with them is formulated as an energy minimization problem allowing incorporation of geometric prior information about the surface to be extracted. However, as the energy function to be minimized usually has several local minima, its minimization is a challenging task. Particularly, the surface extraction result often depends highly on the initialization for the process limiting automatic application of deformable models. In this study, we have minimized the energy of the deformable model globally either with the DSM algorithm or the DSM-OS algorithm. For extraction of the brain surface where it is favorable to approach the surface of interest from outside, we applied the DSM-OS algorithm capable of taking advantage of such prior knowledge. The standard DSM algorithm was applied for extraction of the white matter surface, where it is hard to specify the best direction to approach the surface of interest. Although also these algorithms feature some sensitivity to their initializations, with them problems with initialization sensitivity are considerably reduced. This allowed us to generate initial surfaces for the algorithms automatically without any references to anatomical images. For this reason extracted surfaces can be applied for registration purposes. Optimization algorithms are also deterministic, which could be important for reproducibility of results. Another important merit of the applied deformable model for this study was that it could be applied to brain surface extraction both from Raclopride and FDG PET images. Moreover, model parameters and the initialization process were the same in both cases, which is of importance for automatic surface extraction. Obviously, since two types of images mentioned are quite divergent, different local image features define the surfaces of interest. Edge following used with FDG images, i.e using image gradients as features of interest, would probably not lead to good results for brain surface extraction from Raclopride images. Designing suitable energy images for them required somewhat more effort. Nevertheless, the computation of energy images for the Raclopride tracer was still quite simple and it did not require assumptions e.g. about the parametric form of the probability density function of image histograms.

The identification of the brain surface and separation of hemispheres are starting points for extraction of other surfaces and structures from the brain image. In this study, we extracted the white matter surface with the DM-DSM method from FDG images after delineation of the brain surface. In a similar way, also other structures visible in images could iteratively be extracted by starting from, for example, regions of the highest uptake of the radiopharmaceutical, or from the largest structures. We have presented the principal idea of this kind of analysis with preliminary results in (Ruotsalainen et al., 2001). The extracted structures

from PET images could be identified and labeled for an automatic regional image analysis. This kind of intelligent procedures for delineation and labeling of several brain structures, either one by one or all in one step, from anatomical images have been considered for example in (Lötjönen et al., 1999; Mangin et al., 1995; McInerney et al., 2002). Regional numerical values, for example regional receptor densities, from functional PET images are needed for evaluation of the proper dose of a new drug. The automatic extraction of volumes of interest from the PET images could help in this task by improving the registration of functional and anatomical images, and by giving reliably the boundaries of a distinct uptake of the radiopharmaceutical. Behaviour of the selected radiopharmaceutical in the tissue of interest is generally known based on cellular level and animal experiments. Based on this expectation, we can provide necessary prior information for designing surface extraction methods with deformable models. More advanced and application specific means to create energy images would also be beneficial for the current task of extracting the cortical structure. In the experiments, no anatomical reference structures from MR images were applied. However, this could be done for example for annotation purposes or also for initialization of the search.

In this study, we designed and tested a fully automatic procedure for delineating the brain surface and the mid-sagittal plane from PET brain images. The procedure is based on the new DM-DSM method, which is tolerant to noise in images. The procedure was tested with a phantom study and human brain studies. The resulting brain surfaces and mid-sagittal planes for these were of excellent quality. Because extraction of the surfaces and the mid-sagittal planes was made without any references to anatomical images they can be used for example for image registration purposes. The procedure provides new ways to automate segmentation of PET images.

Acknowledgements

The authors would like to thank the *Turku PET Centre* for providing PET images for evaluation. This study was financially supported by Tampere Graduate School in Information Science and Engineering (TISE), Academy of Finland and Tekes (Drug2000 Technology Program).

References

Alenius, S., Ruotsalainen, U., 2002. Generalization of median root prior reconstruction. IEEE Transactions on Medical Imaging 21 (11), 1413–1420.

Alenius, S., Ruotsalainen, U., Astola, J., 1998. Using local median as the location of the prior distribution in iterative emission tomography image reconstruction. IEEE Transactions on Nuclear Science 45 (6), 3097–3105.

Ardekani, B., Braun, M., Hutton, B., Kanno, I., Iida, H., 1995. A fully automatic multimodality image registration algorithm. Journal of Computer Assisted Tomography 19 (4), 615–623.

Ardekani, B., Kershaw, J., Kanno, M. B. I., 1997. Automatic detection of the mid-sagittal plane in 3-d brain images. IEEE Transactions on Medical Imaging 16 (12), 947 954.

Bardinet, E., Cohen, L., Ayache, N., July 1998. A parametric deformble model to fit unstuctured 3D data. Computer Vision And Image Understanding 71 (1), 39 – 54.

Besl, P., McKay, N., 1992. A method for registration of 3-D shapes. IEEE Transactions on Pattern Analysis and Machine Intelligence 14 (2), 239–256.

Cohen, L., Cohen, I., November 1993. Finite-element method for active contour models and balloons for 2-D and 3-D images. IEEE Transactions on Pattern Analysis and Machine Intelligence 15 (11), 1131 – 47.

Davatzikos, C., Bryan, N., 1996. Using a deformable surface model to obtain a shape representation of the cortex. IEEE Transactions on Medical Imaging 15 (6), 785–795.

Debreuve, E., M. Barlaud, G. A., Laurette, I., Darcourt, J., 2001. Space-time segementation using level set active contours applied to myocardial gated spect. IEEE Transactions on Medical Imaging 20 (7), 643 – 659.

Delingette, H., 1999. General object reconstruction based on simplex meshes. International Journal of Computer Vision 32, 111–142.

Gunn, R., Lammertsma, A., Hume, S., Cunningham, V., 1997. Parametric imaging of ligand-receptor binding in PET using a simplified reference region model. Neuroimage 6, 279–287.

Heijmans, H. A., June 1991. Theoretical aspects of gray-level morphology. IEEE Transactions on Pattern Analysis and Machine Intelligence 13 (6), 568–582.

Huesman, R., Klein, G., Reutter, B., Teng, X., 1998. Multiscale PET quantitation using three-dimensional volumes of interest. In: Carson, R. E., Herscovitch, P., Daude-Witherspoon, M. (Eds.), Quantitative Functional Brain Imaging with Positron Emission Tomography. Academic Press, Ch. 8, pp. 51–58.

Hutton, B., Braun, M., Thurfjell, L., Lau, D., January 2002. Image registration: an essential tool for nuclear medicine. European Journal of Nuclear Medicine 29 (4), 559–577.

Kass, M., Witkin, A., Terzopoulos, D., 1987. Snakes: Active contour models. International Journal of Computer Vision 1, 321–331.

Klein, G., Huesman, R., 2002. Four-dimensional processing of deformable cardiac PET data. Medical Image Analysis 6 (1), 29–46.

Lai, K., Chin, R., 1995. Deformable contours - modelling and extraction. IEEE Transactions on Pattern Analysis and Machine Intelligence 17 (11), 1084 – 1090.

Liu, Y., Collins, R., Rothfus, W., 2001. Robust midsagittal plane extraction from normal and pathological 3-D neuroradiology images. IEEE Transactions on Medical Imaging 20 (3), 175–192.

Lötjönen, J., Reissman, P.-J., Magnin, I., Katila, T., 1999. Model extraction from magnetic resonance volume data using the deformable pyramid. Medical Image Analysis 3 (4), 387–406.

Luoma, J., May 25-28 2002. Extracting hemisphere structures automatically from brain PET images. In: Knuuti, J., Någren, K. (Eds.), Abstracts of the IX Turku PET Symposium. No. D 499 in Annales Universitatis Turkuensis. University of Turku, p. Q4.

MacDonald, D., Kabani, N., Avis, D., Evans, A., 2000. Automated 3-D extraction of inner and outer surfaces of cerebral cortex from MRI. NeuroImage 12 (3), 340–358.

Malladi, R., Sethian, J., Vemuri, B. C., February 1995. Shape modelling with front progagation: A level set approach. IEEE Transactions on Pattern Analysis and Machine Intelligence 17 (2), 158 – 175.

Mangin, J.-F., Tupin, F., Frouin, V., Bloch, I., Rougetet, R., Regis, J., Lopez-Krahe, J., 1995. Deformable topological models for segmentation of 3D medical images. In: Proc. of Information Processing in Medical Imaging, IPMI95. pp. 153–164.

McInerney, T., Hamarneh, G., Shenton, M., Terzopoulos, D., 2002. Deformable organisms for automatic medical image analysis. Medical Image Analysis 6 (3), 251–266.

McInerney, T., Terzopoulos, D., 1996. Deformable models in medical image analysis: a survey. Medical Image Analysis 1 (2), 91–108.

Mykkänen, J., Juhola, M., Ruotsalainen, U., 2000. Extracting VOIs from brain PET images. International Journal of Medical Informatics 58-59, 51–57.

Mykkänen, J., Tohka, J., Ruotsalainen, U., 2001. Automated delineation of brain structures with snakes in PET. In: Gjedde, A., Hansen, S., Knudsen, G. M., Paulson, O. (Eds.), Physiological Imaging of the Brain with PET. Academic Press, pp. 39–43.

Mykkänen, J., Tohka, J., Ruotsalainen, U., 2003. Delineation of brain structures from positron emission tomography images using deformable models. In: Baud, R., Fieschi, M., Le Beaux, P., Ruch, P. (Eds.), The new navigators: from professionals to patients. Vol. 95. IOS Press, pp. 33–38.

Noumeir, R., El-Daccache, R., 1998. Attenuation correction in spect using active surfaces. In: Proc. of IEEE-Nuclear Science Symposium 1998. Vol. 3. pp. 1995 – 1999.

Prima, S., Oursein, S., Ayache, N., 2002. Computation of the mid-sagittal plane in 3-D brain images. IEEE Transactions on Medical Imaging 21 (2), 122–138.

Rousseeuw, P., Leroy, A., 1987. Robust Regression and Outlier Detection. Wiley-Interscience, New York.

Ruotsalainen, U., 1997. Quantification and data analysis in positron emission tomography: organ blood flow, graphical analysis and radiation dosimetry. Ph.D.

thesis, Tampere University of Technology Publications 224.

Ruotsalainen, U., Mykkänen, J., Luoma, J., Tohka, J., Alenius, S., 2001. Methods to improve repeatability in quantification of brain PET images. In: World Congress on Neuroinformatics. ARGESIM Report 20. ARGESIM/ASIM Verlag Vienna, pp. 659–664.

Shen, D., Herskovits, E., Davatzikos, C., April 2001. An adaptive focus statistical shape model for segmentation and shape modeling of 3D brain structures. IEEE Transactions on Medical Imaging 20 (4), 257 – 270.

Tohka, J., 2002. Surface extraction from volumetric images using deformable meshes: A comparative study. In: Proc. of 7th European Conference on Computer Vision. No. 2352 in Lecture Notes in Computer Science. pp. 350 – 364.

Tohka, J., Mykkänen, J., 2003. Deformable mesh for automated surface extraction from noisy images, accepted for publication in the Special Issue on Deformable models for Image Analysis and Pattern Recognition for *International J. of Image and Graphics*.
URL `http://www.cs.tut.fi/~jupeto/dmnoisy.pdf`

Vaillant, M., Davatzikos, C., 1997. Finding parametric representation of the cortical sulci using an active contour model. Medical Image Analysis 1 (4), 295–315.

Williams, D., Shah, M., 1992. A fast algorithm for active contours and curvature estimation. CVGIP: Image Understanding 55 (1), 14–26.

Woods, R., Mazziotta, J., Cherry, S., 1993. Automated image registration. In: Uemura, K., Lassen, N., Jones, T., Kanno, I. (Eds.), Quantification of Brain Function, Tracer Kinetics and Image Analysis in Brain PET. Excerpta Medica, pp. 391–398.

Xu, C., Pham, D., Rettmann, M., Yu, D., Prince, J., 1999. Reconstruction of the human cerebral cortex from magnetic resonance images. IEEE Transactions on Medical Imaging 18 (6), 467–479.

Xu, C., Prince, J., 1998. Generalized gradient vector flow external forces for active contours. Signal Processing 71 (2), 131 – 139.

Zeng, X., Staib, L., Schultz, R., Duncan, J., 1999. Segmentation and measurement of the cortex from 3-D MR images using coupled-surfaces propagation. IEEE Transactions on Medical Imaging 18 (10), 927–937.

Zhang, Z., 1994. Iterative point matching for registration of free-form curves and surfaces. International Journal of Computer Vision 13 (2), 119 – 152.

Zucker, S., Hummel, R., 1981. A three-dimensional edge operator. IEEE Transactions on Pattern Analysis and Machine Intelligence 3 (3), 324–331.

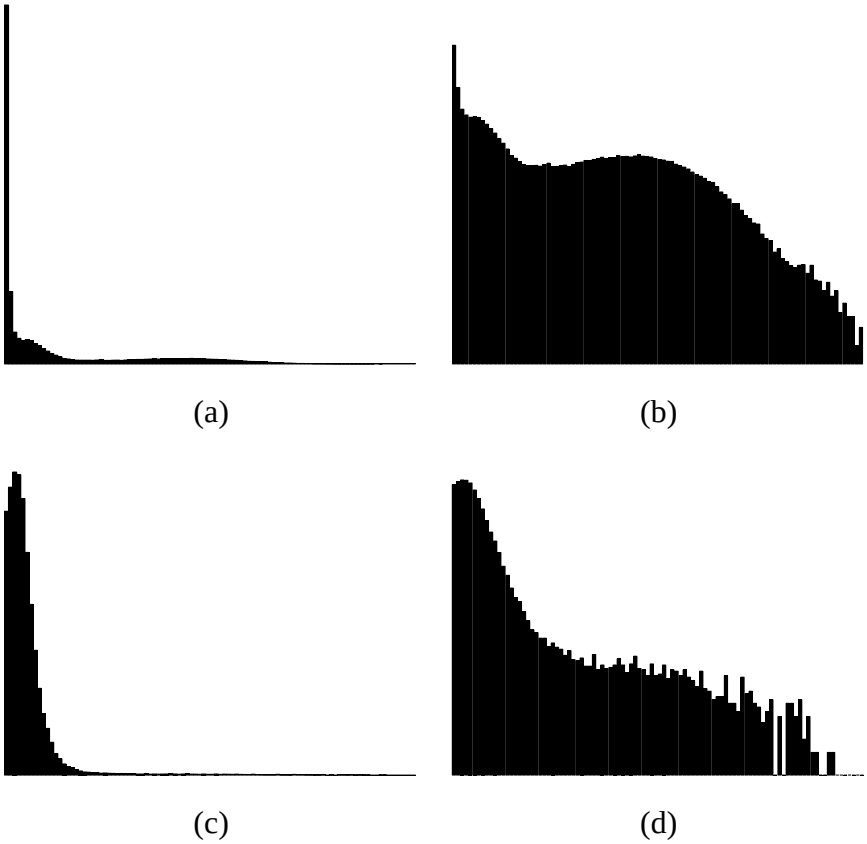

Fig. 1. The histogram of an image from FDG-PET study with (a) linear scaling and (b) logarithmic scaling and from Raclopride study with (c) linear scaling and (d) logarithmic scaling. Intensity values equaling zero are not included in the histograms.

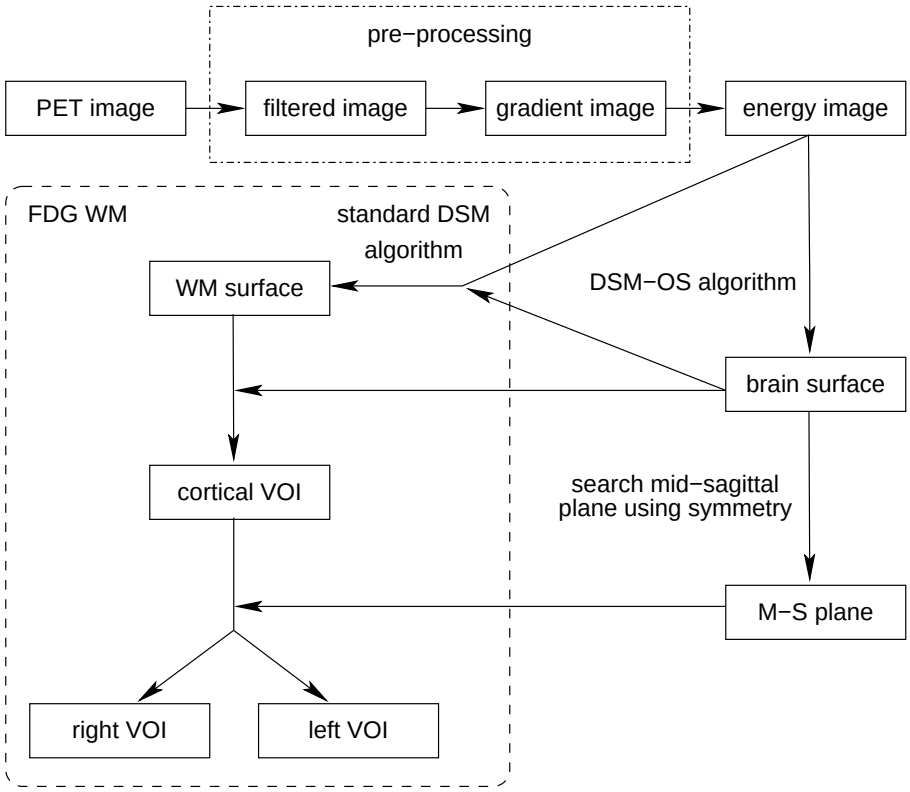

Fig. 2. Surface extraction and determination of volumes of interest (VOIs) automatically from PET brain images using the DM-DSM method and the mid-sagittal (M-S) plane. The white matter surface and cortical VOIs are only extracted from images from FDG-PET studies.

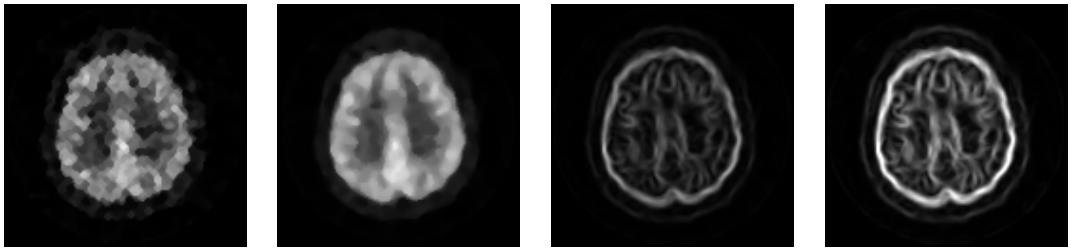

(a) (b) (c) (d)

Fig. 3. Steps in energy image computation in the case of FDG-PET brain images. Transaxial image cross-sections from (a) the original image, (b) the median filtered image, (c) the gradient image and (d) the energy image, which is a contrast enhanced version of the gradient image in (c).

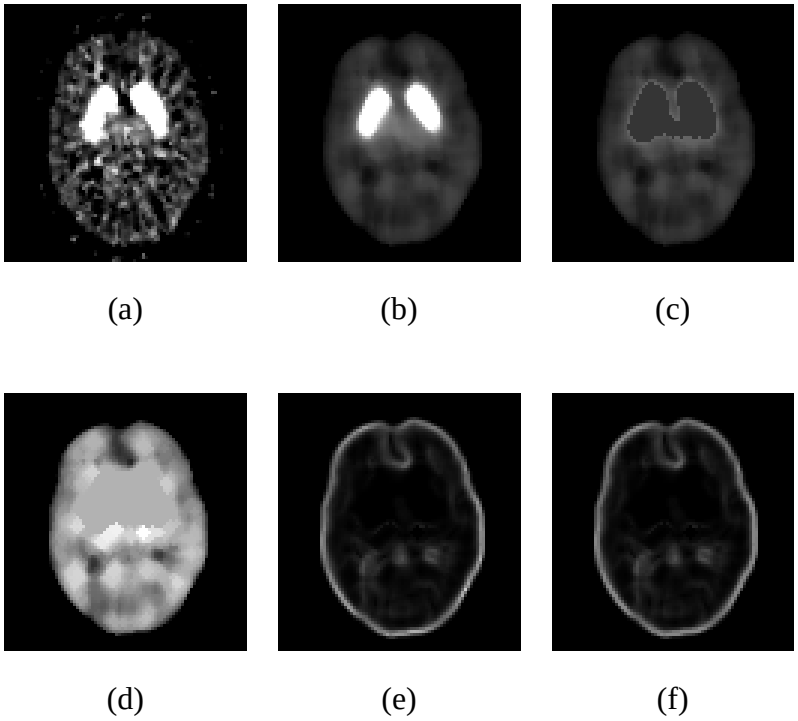

Fig. 4. Steps in energy image computation in the case of ^{11}C-Raclopride brain images. Transaxial image cross-sections from (a) the original image, (b) the median filtered image, (c) the image where high intensity values in striatum have been replaced by the average intensity value of the image, (d) the image after morphological filtering, (e) the energy image before contrast enhancing normalization and (f) the energy image. In (a) and (b) highest intensity values (in striatum) have been scaled down in order to make low intensity values elsewhere in the brain volume visible.

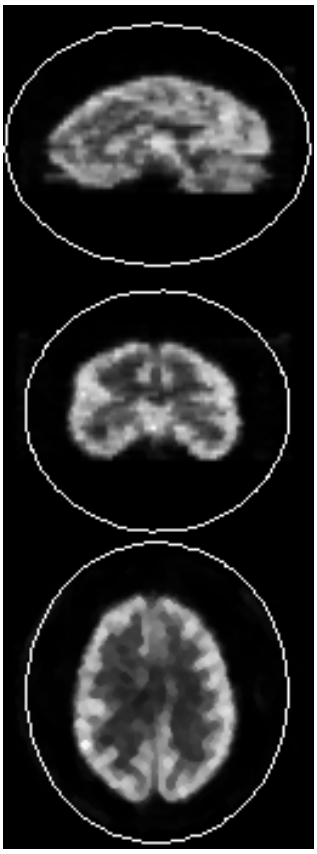

Fig. 5. Automatically generated initialization for the search of the brain surface shown on the PET image. From top, sagittal, coronal and transaxial cross-section views.

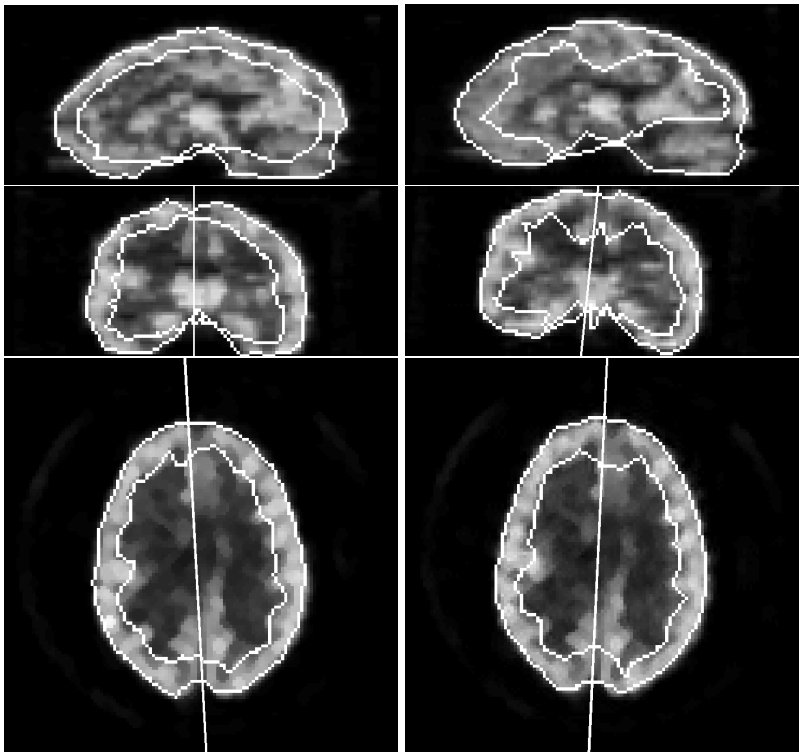

Fig. 6. The brain surface, white matter surface and mid-sagittal plane extracted from the original and the rotated Hoffman phantom image.

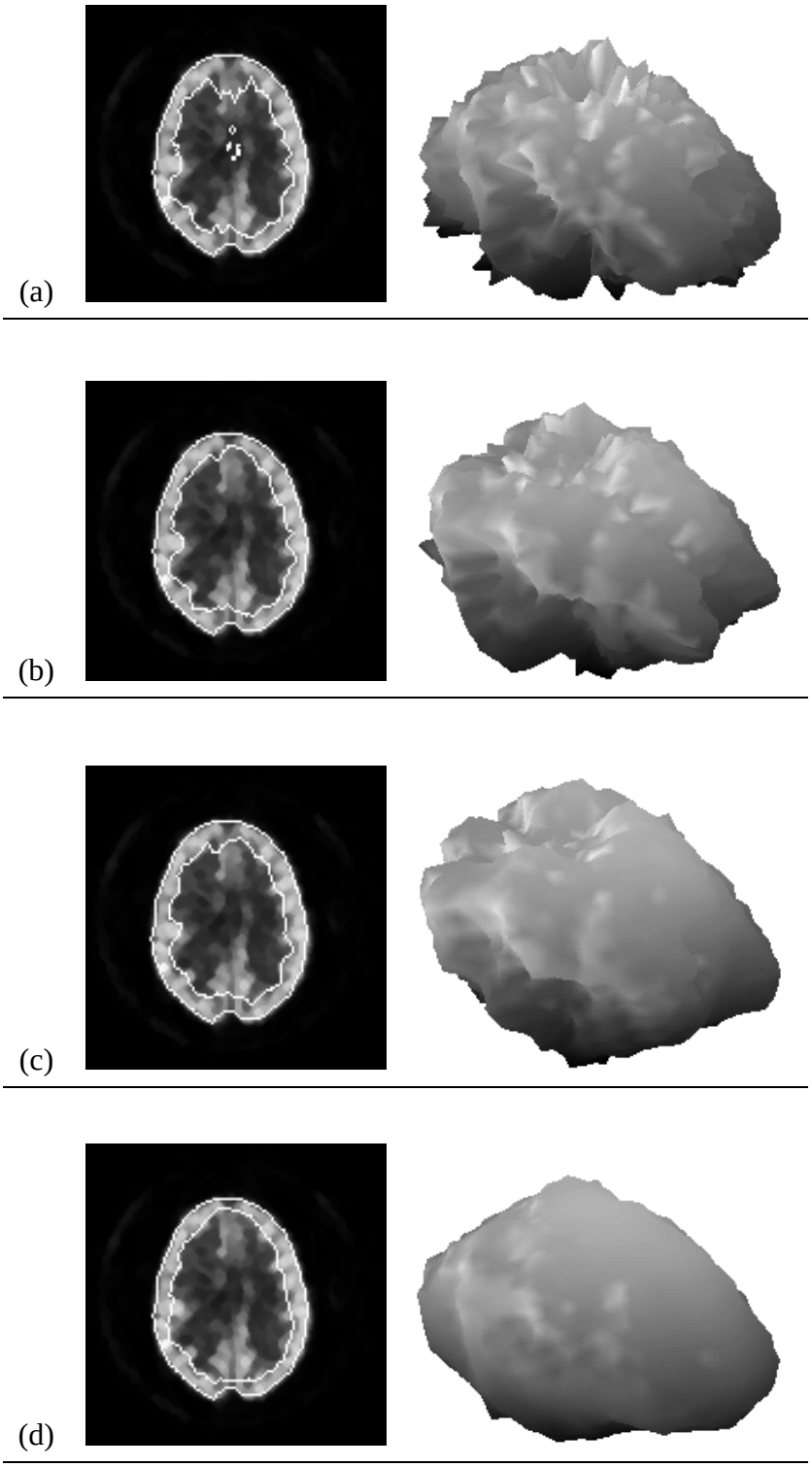

Fig. 7. The effect of the amount of the regularisation in searching of the white matter surface with the Hoffman phantom: (a) λ is zero , (b) $\lambda = 0.05$, (c) $\lambda = 0.2$ and (d) $\lambda = 0.5$. A transaxial cross-section is shown on the left column and a three-dimensional rendering is shown on the right column. The smoothness of the mesh could not be controlled without shape regularisation as shown in (a). The brain surface shown on the transaxial cross-sections is the same in all cases.

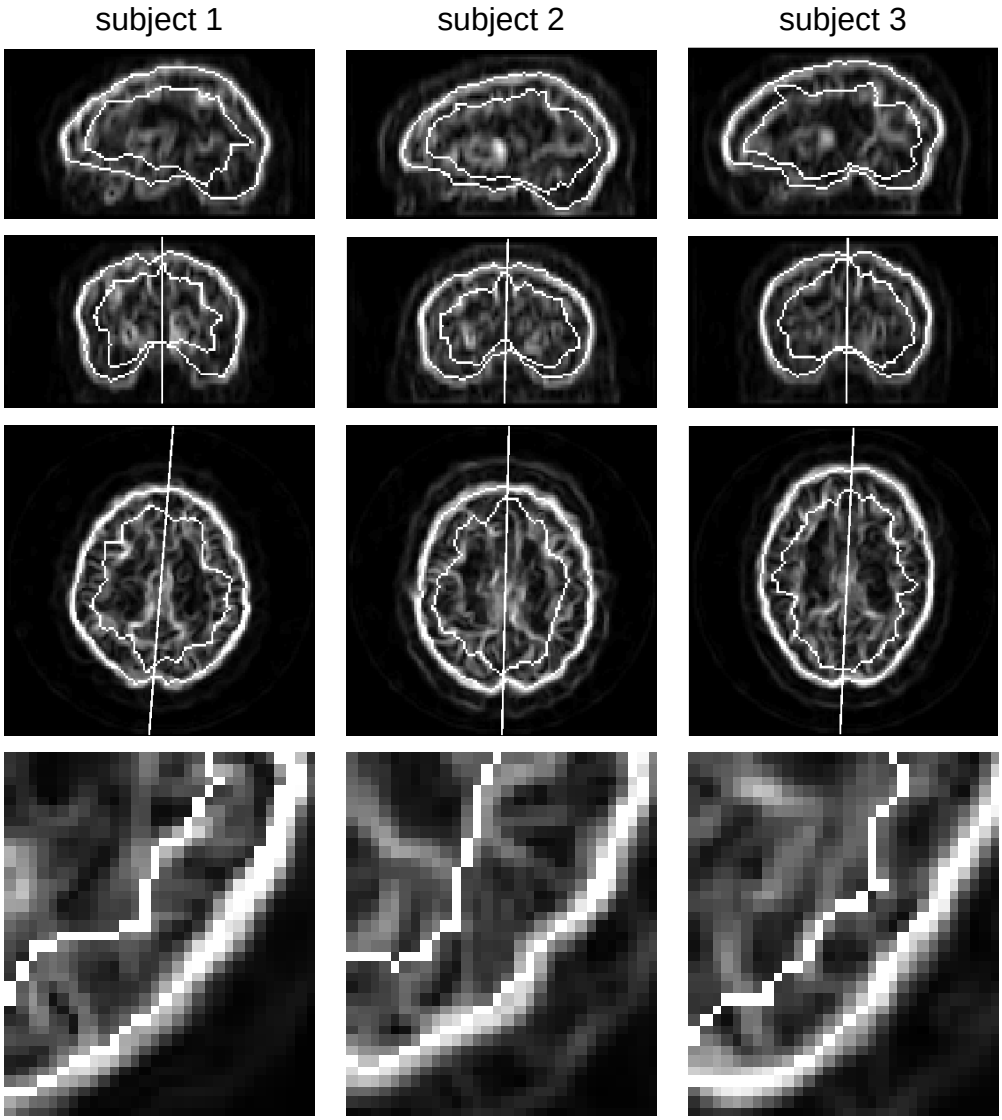

Fig. 8. Examples of automatically delineated brain surfaces, mid-sagittal planes, and white matter surfaces from FDG-PET brain images of overlayed on the energy image. Based on the visual quality of the white matter surfaces, subject 1 is the best result, subject 2 represents a typical result and subject 3 is the worst result, cf. the text. From top, sagittal, coronal and transaxial cross-section views. The mid-sagittal plane is marked only on the coronal and the transaxial cross-sections. Bottom, magnifications (500 %) of the lower right corner of the transaxial image cross-section are shown.

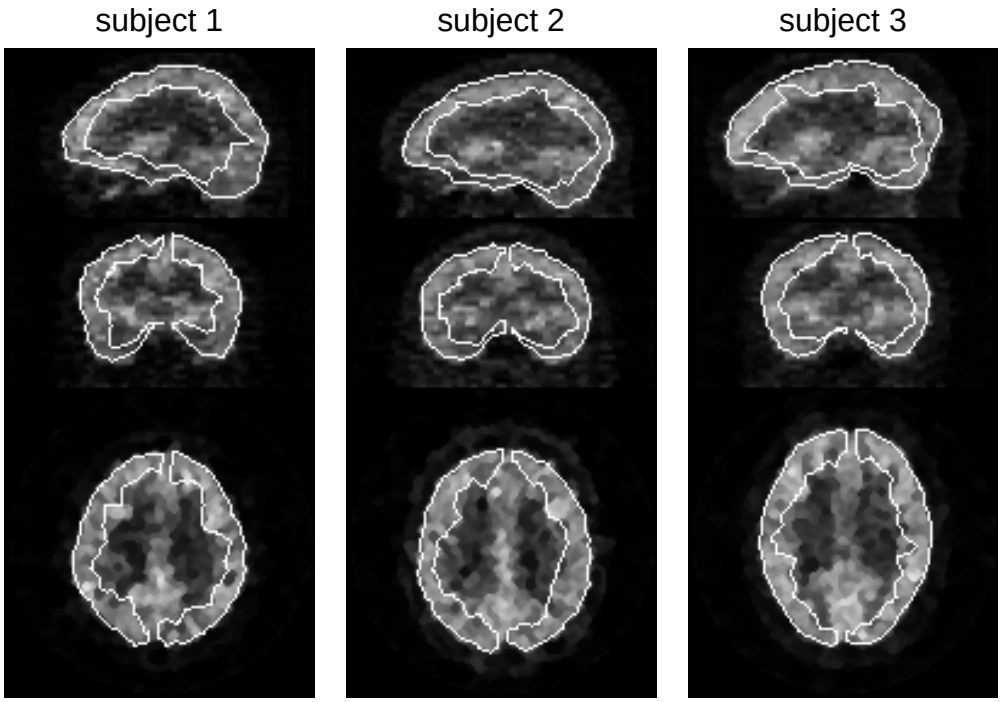

Fig. 9. The extracted VOIs overlayed on the original FDG-PET images.

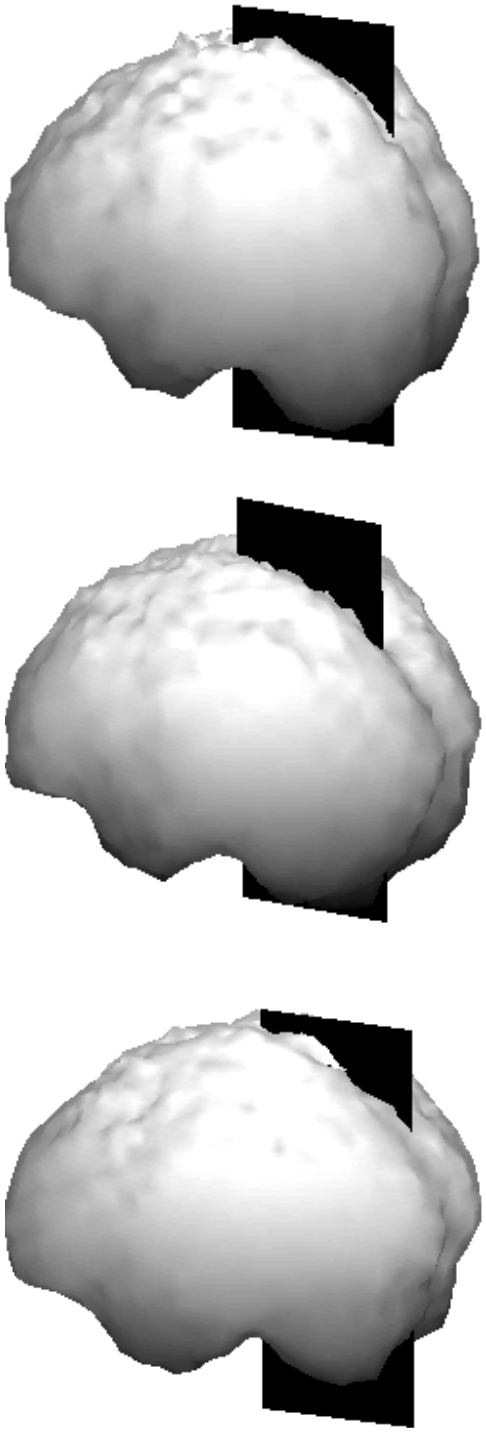

Fig. 10. Three-dimensional renderings of brain surface meshes extracted from the FDG-PET brain images. The determined mid-sagittal planes are shown on black. From top, subject 1, subject 2 and subject 3.

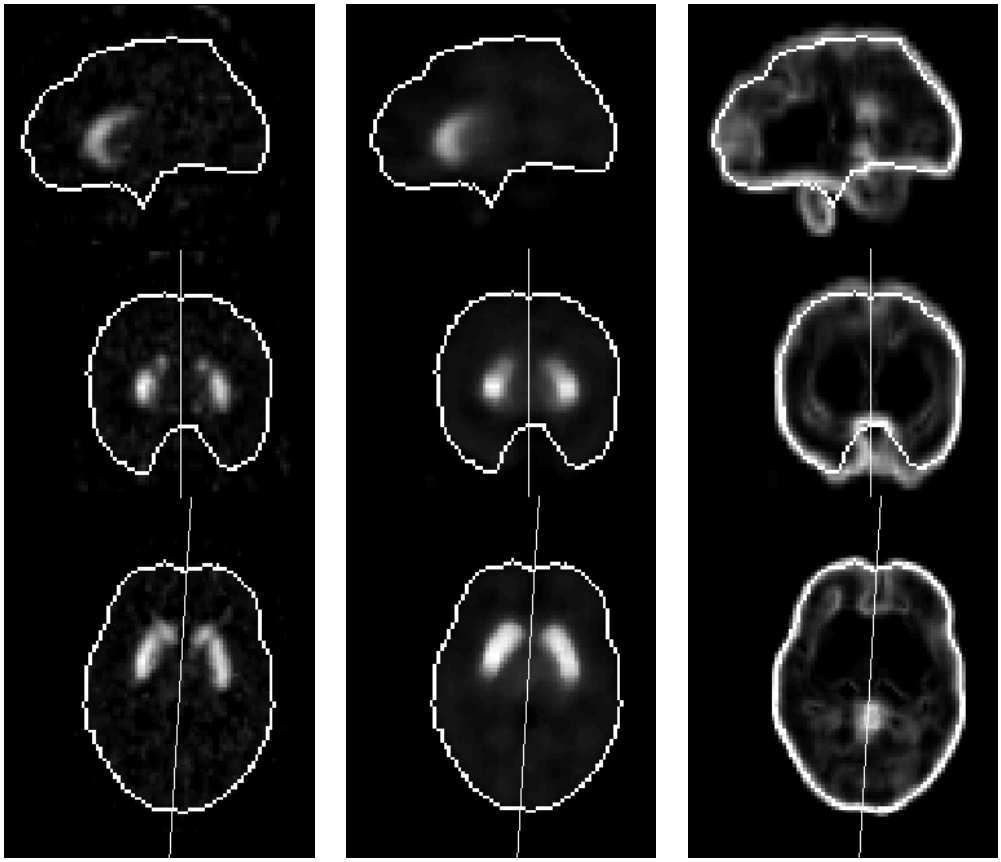

(a) (b) (c)

Fig. 11. Extracted brain surface and mid-sagittal plane from a Raclopride brain image overlayed on (a) the original image, (b) the median filtered image and (c) the energy image. From top, sagittal, coronal and transaxial cross-section views.